ACS OMEGA

http://pubs.acs.org/journal/acsodf
Article

Are 3D Tumor Cell Spheroids a Utile System for the In Vitro Evaluation of Diagnostic Radiotracers?

Benedikt Judmann,[#] Florian Keller,[#] Björn Wängler, Ralf Schirrmacher, Rüdiger Rudolf, and Carmen Wängler*

Cite This: *ACS Omega* 2024, 9, 51349−51362

ABSTRACT: By possibly bridging the gap between 2D *in vitro* cell assays and *in vivo* applications, tumor cell spheroid cultures offer promising avenues for advancing innovation in nuclear medicine. Regarding the *in vitro* evaluation of therapeutic radioligands, tumor cell spheroids have been successfully used to assess the therapeutic efficacy against human tumors. However, studies employing spheroids for testing diagnostic tracers are missing. The present work investigated the receptor interaction of a diagnostic radioligand with different tumor cell spheroids and compared the results to those received from a standard 2D cell assay to validate the usefulness of 3D cell systems for diagnostic radiotracer testing. For this purpose, a new agent—[^{68}Ga]Ga-NODAGA-PEG$_5$-c(RGDfK)—was developed. In competitive displacement assays against [^{125}I]I-echistatin in human U87MG glioblastoma cell monolayers, NODAGA-PEG$_5$-c(RGDfK) demonstrated specific binding and IC_{50} values of 3.08 ± 0.12 and 10.39 ± 0.89 μM in the absence and presence of basal membrane extract (BME), respectively. Compared to cell monolayers, the 3D cell aggregates yielded considerably higher IC_{50} values of 16.46 ± 2.88, 20.52 ± 4.41, and 18.44 ± 6.06 μM in spheroids generated without additive, collagen-1, and BME supplementation and showed considerable unspecific binding. The obtained data were contextualized by investigating differences in morphology, cell viability, and integrin content per cell of the 2D and 3D cell models as well as the influence of ECM composition. Integrin expression per cell was stable, while spheroid density and the associated radioligand uptake were varying, depending on the culture conditions. This suggests a correlation between the NODAGA-PEG$_5$-c(RGDfK)-integrin $\alpha_v\beta_3$-interaction and cell model compactness. Further, a considerable influence of matrix components on ligand−receptor interaction could be demonstrated. Overall, the results showed profound differences between the 2D and 3D radiotracer assays investigated, and further work is warranted to verify the expected added value of 3D tumor cell spheroids for the evaluation of diagnostic radioligands.

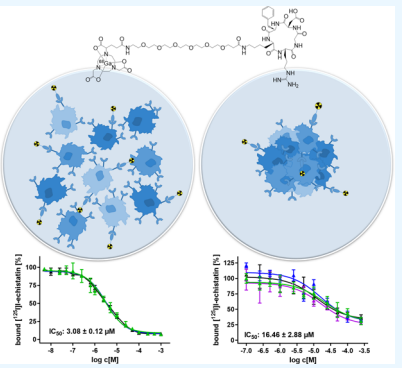

INTRODUCTION

Diagnostic radiolabeled agents are an important class of pharmaceuticals being systemically administered to patients in order to visualize human malignancies by means of positron emission tomography (PET) or single photon emission computed tomography (SPECT). Moreover, radiopharmaceuticals can also be used for therapeutic purposes when a therapeutic radionuclide is applied instead of a diagnostic one.

Due to their high importance in nuclear medicine imaging and therapy of malignant diseases, a great plethora of tumor-specific radioligands has been developed over the last decades.[1,2] For this purpose, bioactive compounds being able to address the tumor-specific target structure (mainly receptors on the tumor cell surface) such as peptides, antibodies, or other bioactive targeting agents derived from them are used as specifically accumulating carriers for the radionuclide of choice. Every newly developed radiopharmaceutical has to undergo extensive testing before being applied to a human subject, as by modification of the target-specific biomolecule with a diagnostic or therapeutic radionuclide, the target binding characteristics of the carrier can be affected. Ideally, the agent should exhibit a high uptake into the tumor while at the same time showing low uptake into and rapid washout from healthy organs and tissues, resulting in high tumor-to-background ratios. For this, a high affinity of the radioligand for the respective tumor-specific target structure is key to its efficient uptake and accumulation in the tumor. Accordingly, this central radiotracer characteristic is routinely determined by performing *in vitro* competitive displacement studies on human tumor cells and is considered a prerequisite for subsequent *in vivo* evaluation of the agents in human tumor-bearing xenografts. These *in vitro* experiments thus enable the

Received: September 6, 2024
Revised: November 8, 2024
Accepted: November 13, 2024
Published: December 16, 2024

https://doi.org/10.1021/acsomega.4c08214
ACS Omega 2024, 9, 51349−51362

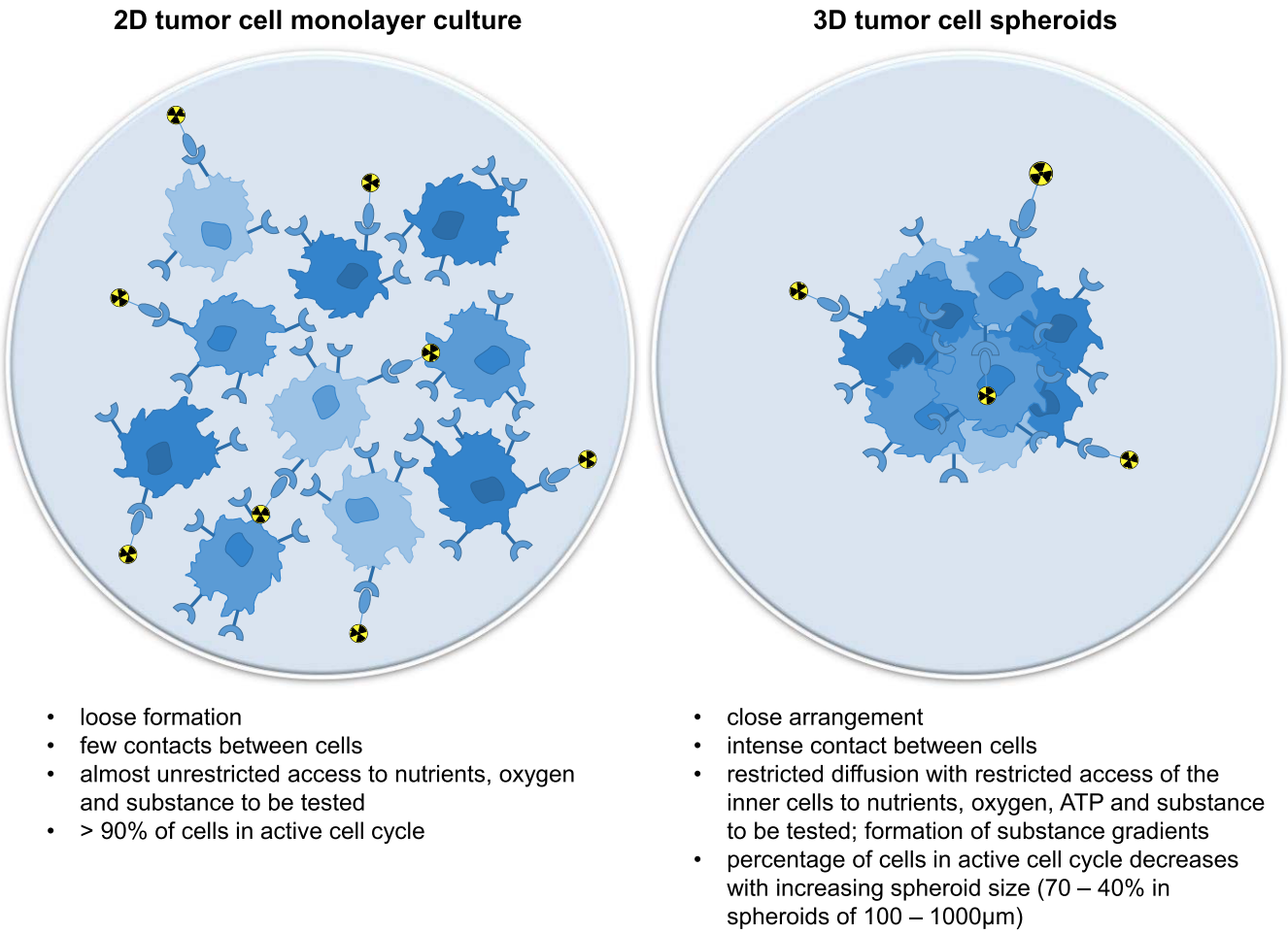

Figure 1. Schematic depiction of the main differences between cancer cells in 2D monolayer cell culture systems and 3D spheroids.

identification of promising radiotracer candidates with high potential for human translation.

Radiotracer-tumor cell interactions and target affinity are commonly studied *in vitro* in 2D monolayer tumor cell systems. These are well standardized, giving highly reproducible and thus comparable results. However, there are some shortcomings associated with 2D cell systems, namely, the lack of cell−cell and cell−extracellular matrix (ECM) interactions.[3] These interactions might considerably influence the interplay of the drug to be evaluated with malignant as well as healthy cells but remain unstudied using conventional 2D tumor cell models for *in vitro* testing. A conceivable way to overcome these limitations is the use of 3D cell systems such as spheroids, organoids, or microfluidic tumor on a chip platforms.[4]

Tumor cell spheroids form by spherical aggregation of tumor cells and thus better reflect the natural spatial organization of human tumor cells and their interaction with the extracellular environment, showing—in contrast to 2D tumor cell models—cell aggregation, proliferation and growth kinetics, differentiation, and cell−cell and cell−ECM interaction.[5] Hence, spheroids can be regarded as a bridging link between 2D *in vitro* cell and 3D *in vivo* animal cancer models allowing for a better representation of the native tumor cell situation (being of high relevance for drug development) than 2D tumor cell systems.[3,6] In the case of radiotherapeutics, these characteristics enable us to determine the treatment efficacy of new drugs more accurately than 2D cell monolayers and thus to identify potential anticancer drugs with a higher predictive value.

Several studies compared the efficiency of therapeutic radiopharmaceuticals to be applied in tumor treatment in 2D vs 3D cancer cell models.[7] It was demonstrated that human tumor cells being organized in 3D spheroids allow for a better assessment of the therapeutic efficacy of the investigated radiotherapeutics due to different factors (Figure 1) as follows.

First, in tumor cell spheroids, the percentage of cells being in active states of the cell cycle gradually decreases with increasing spheroid size of 100−1000 μm to 70−40%, whereas tumor cells in 2D models show cycling rates of more than 90%.[8] The 3D model thus reflects much better the *in vivo* situation than cell monolayers and reduced cycling rates explain the generally less pronounced therapeutic effects of radiotherapeutics being observed in tumor spheroids compared to tumor cell monolayers.[7] Further factors expounding these differences are altered gene expression profiles of genes regulating biological processes like tissue development, cell adhesion, immune system, and defense response in 3D compared to tumor cell monolayers, resulting in a decreased cellular responsiveness to external stress such as ionizing radiation in spheroids.[9] Although these factors usually result in a lower response of the cancer cells in 3D spheroids to the tested radiotherapeutics, this is not a drawback, as it better reflects the real *in vivo* tumor situation and thus allows a better assessment of the efficacy of the compounds in the living organism than 2D cell models.

https://doi.org/10.1021/acsomega.4c08214
ACS Omega 2024, 9, 51349−51362

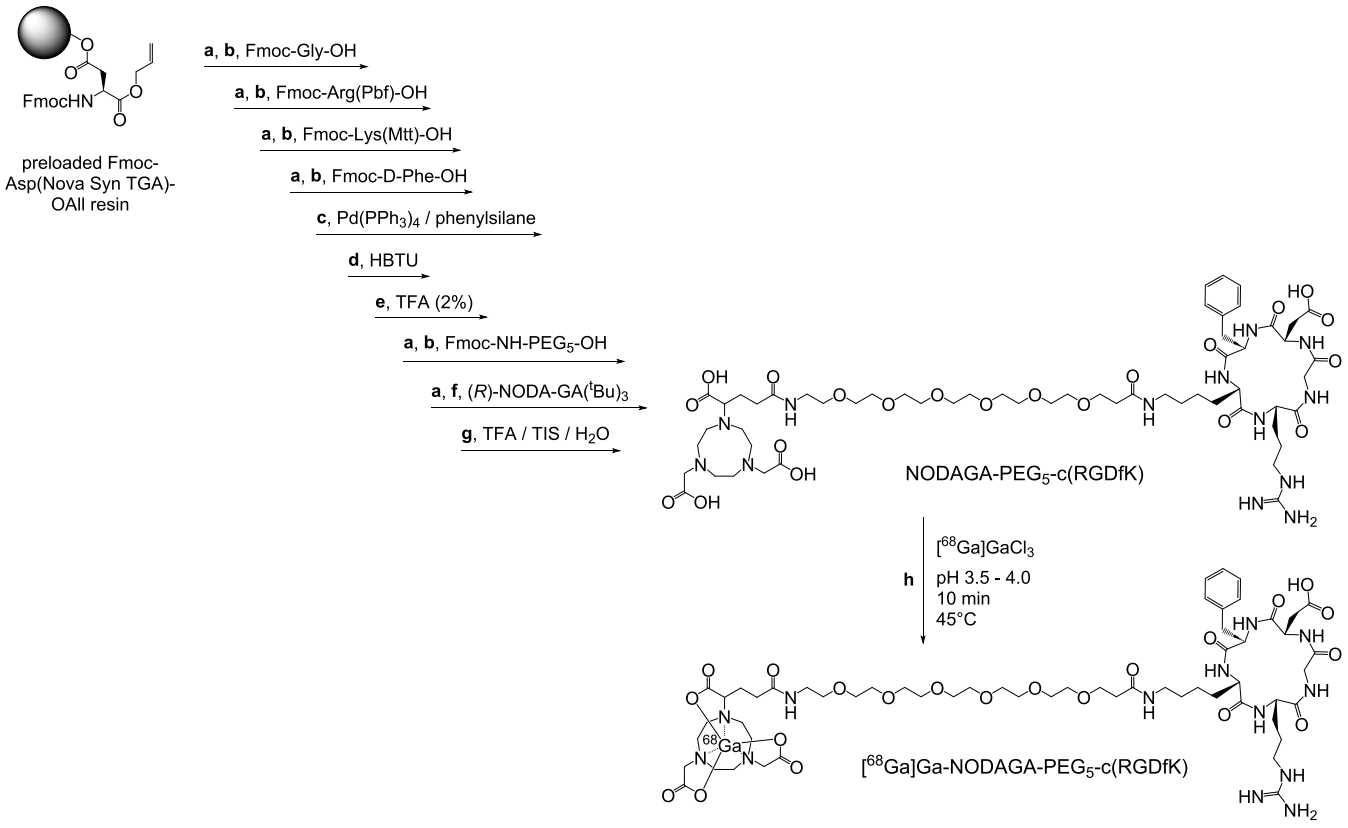

Figure 2. Synthesis route and structure of the peptidic labeling precursor molecule NODAGA-PEG$_5$-c(RGDfK) and its subsequent radiolabeling with $^{68}Ga^{3+}$. Conditions: (a) cleavage of Fmoc-protecting group: piperidine/DMF (1:1, *v*/*v*), 2 + 5 min; (b) activation of amino acid: 2.0 equiv amino acid derivative, 2.0 equiv DIPEA, 1.9 equiv HBTU in DMF, 2 min, 15 min conjugation using ultrasound assistance; (c) *O*-allyl-deprotection: 0.25 equiv $Pd(PPh_3)_4$, 24 equiv phenylsilane, DCM, 3 × 30 min; (d) cyclization: 1 equiv. HBTU in DMF, 1 h ultrasonication; (e) Mtt-removal: TFA in DCM (2% (*v*/*v*)), 5 × 5 min; (f) activation of chelator: 2.0 equiv chelator, 2.0 equiv DIPEA, 1.9 equiv PyBOP in DMF, 2 min, 30 min conjugation using ultrasound assistance; (g) cleavage of peptide from resin and simultaneous deprotection of side chain functional groups: TFA/TIS/H_2O (95:2.5:2.5, *v*/*v*/*v*) for 3 h—followed by purification via HPLC and lyophilization; (h) radiolabeling reaction with $^{68}Ga^{3+}$: 1−20 nmol NODAGA-PEG$_5$-c(RGDfK), 50−380 MBq [^{68}Ga]$GaCl_3$, pH 3.5−4.0, 10 min, 45 °C.

Despite these advantages of tumor spheroids for the evaluation of therapeutic radioligands, similar comparative studies of these 3D *in vitro* test systems are lacking for diagnostic radiopharmaceuticals. Although radiodiagnostics have already been investigated with regard to their uptake in tumor cell spheroids, the binding characteristics of these agents were not in the focus of these studies. Instead, radiotracer uptake was only used as a vehicle to characterize the spheroids.[7]

The testing of new radiotracers in a 3D tumor spheroid model could, however, for the reasons outlined above, be also advantageous for the screening and selection of diagnostic radiolabeled agents and not only for their therapeutic counterparts. In particular, selecting the most suitable compounds from a larger group of new radioligands for further *in vivo* testing is often difficult when all substances under investigation exhibit similar tumor cell interaction profiles and target affinities in 2D *in vitro* test systems. Cancer cell spheroids could add valuable information here and thus be better suited to identify the best candidates for further *in vivo* testing than 2D tumor cell models. Further, 3D tumor cell spheroids could, together with organoids of healthy organs and tissues, be useful as *in vitro* test system, mimicking the most relevant tissues present in a living organism. By this, such a multitissue system might allow a better assessment of the potential of a diagnostic radiopharmaceutical for clinical translation. However, own preliminary and unpublished work in this field led us to the insight that before the setup of such a complex multitissue system is reasonable, the tumor cell spheroids themselves should be characterized systematically in order to assess their usefulness for incorporating them into such complex organ/tissue systems. This involves the assessment of potential diffusion constraints but also the spatial distribution and accessibility of target structures within the spheroid structures.

Therefore, the present study investigated to what extent 3D tumor cell spheroids are suitable to provide additional and reproducible information compared to conventional 2D-based tumor cell systems for the evaluation of the receptor-targeting characteristics of a model radioligand and thus allow a more accurate prediction if a diagnostic radiotracer is suitable for further *in vivo* testing than *in vitro* testing in 2D tumor cell models alone. On the one hand, this would necessitate the 3D tumor cell spheroids to yield highly reproducible results. Furthermore, it also has to be investigated to what extent the matrix used to generate the spheroids, the morphology, and receptor expression in the three-dimensional systems influence the obtained results.

RESULTS AND DISCUSSION

In order to assess the applicability of tumor cell spheroids for the evaluation of diagnostic radioligands in a model system, an

https://doi.org/10.1021/acsomega.4c08214
ACS Omega 2024, 9, 51349−51362

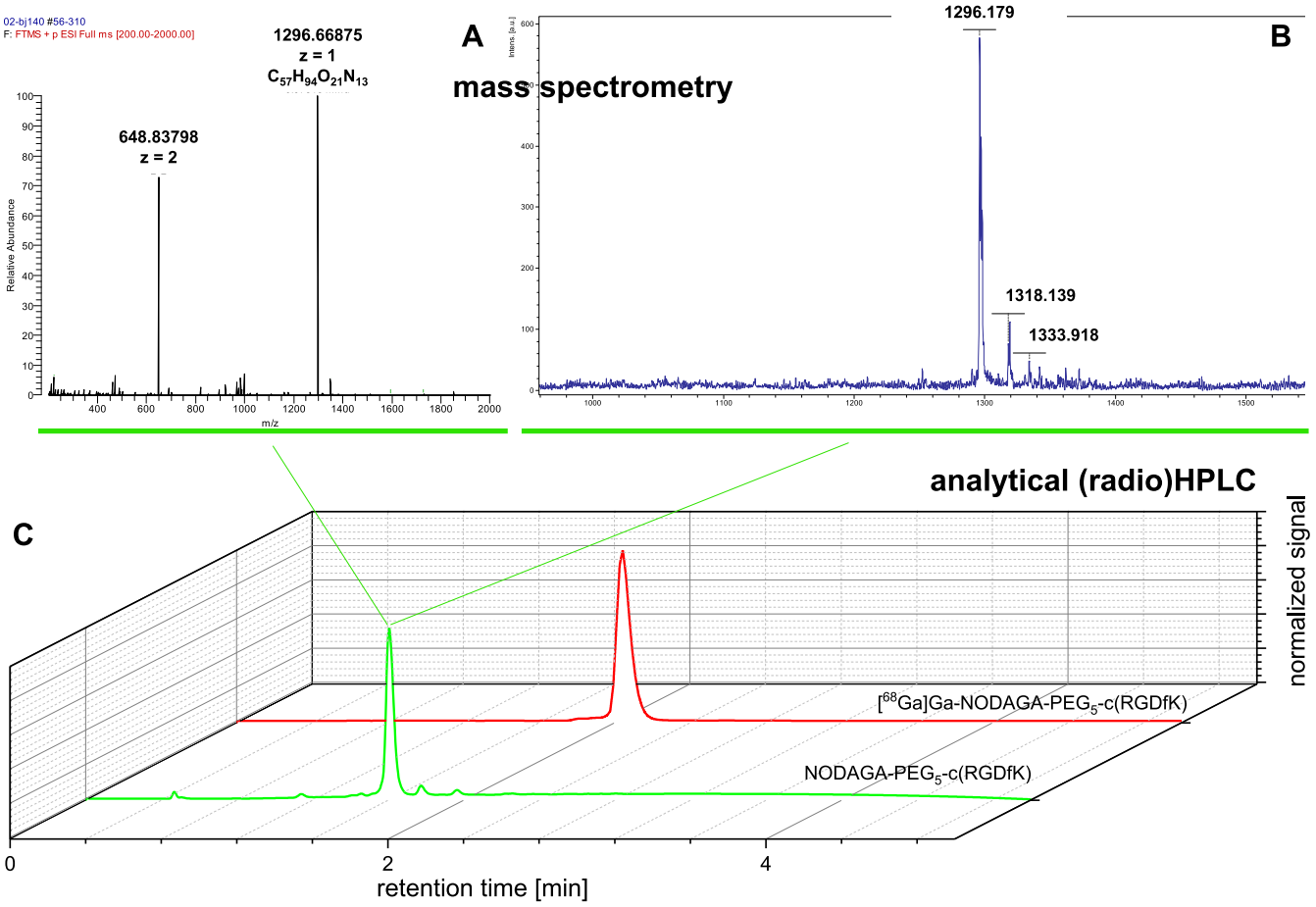

Figure 3. Analytical data for NODAGA-PEG$_5$-c(RGDfK) (green analytical HPLC trace (C) and MALDI (B) and HR-ESI mass spectrometry data (A)) and [^{68}Ga]Ga-NODAGA-PEG$_5$-c(RGDfK) (red analytical radio-HPLC trace (C)).

integrin $\alpha_v\beta_3$-specific radiotracer was developed and evaluated in different *in vitro* test systems regarding its integrin receptor-specific binding characteristics. To avoid a presumptive intrinsic bias resulting from diffusion constraints of a large protein-based radioligand such as a radioimmunoconjugate, the aim was to create a small-sized peptidic tracer. For this purpose, the new chelator-modified and ^{68}Ga-labeled RGD peptide [^{68}Ga]Ga-NODAGA-PEG$_5$-c(RGDfK) (Figure 2) was developed. Radiotracers based on the RGD scaffold binding to integrin $\alpha_v\beta_3$ are important agents for the imaging of tumor angiogenesis,[10,11] thus providing complementary information to PET imaging using [^{18}F]FDG.[12] Another reason for choosing this particular system as the model for the planned direct comparison of *in vitro* tumor cell systems is that the evaluation of new RGD peptide-based radioligands on integrin $\alpha_v\beta_3$-overexpressing tumor cells with regard to cellular interaction and target affinity is very well standardized[13] and lends itself to be compared to a spheroid-based test system.

One aspect of this study was to investigate the extent to which the cellular expression of integrin $\alpha_v\beta_3$ changes during the transfer of the tumor cells from a 2D monolayer to a spheroidal 3D culture and how it is affected by different cell supplementations used for spheroid generation, influencing the results obtained. Although there are indications in the literature that the expression of integrin $\alpha_v\beta_3$ does not change in the case of fibroblasts and breast cancer cells being transferred from 2D to 3D cell culture (in contrast to integrin $\alpha_5\beta_1$, whose expression was shown to be upregulated under these conditions),[14,15] this situation could be different for the integrin $\alpha_v\beta_3$-positive U87MG glioblastoma cells used here. Further, integrin $\alpha_v\beta_3$ also mediates cell−cell interactions, which could be intensified upon translation to a 3D cell spheroid culture. We thus aimed to also investigate the extent to which the results of the *in vitro* evaluations are influenced by the transfer of the cells from 2D to 3D systems and by the alterations of the tumor cells themselves.

Peptide Synthesis, Chelator Modification, and Radiolabeling with ^{68}Ga. The synthesis of the peptidic labeling precursor NODAGA-PEG$_5$-c(RGDfK) was carried out using standard Fmoc strategy-based solid phase-assisted peptide synthesis protocols relying on the sequential conjugation of the respective protected amino acid derivatives (or other, e.g., artificial synthons) to a functional group or amino acid immobilized on a solid support (Figure 2).[16,17] This approach allows for the consecutive assembly of the target peptide on the solid phase. At this stage, the peptide still comprises protecting groups, masking the side chain functionalities of the amino acids. When the target molecule was completely assembled, it was cleaved from the solid support under harsh acidic conditions, which also removed the acid-labile protecting groups of the amino acid side chain functionalities. By this, the product was readily obtained after HPLC purification and its identity and purity were confirmed by HR-ESI (Figure 3A) and MALDI (Figure 3B) mass spectrometry as well as analytical HPLC (Figure 3C).

https://doi.org/10.1021/acsomega.4c08214
ACS Omega 2024, 9, 51349−51362

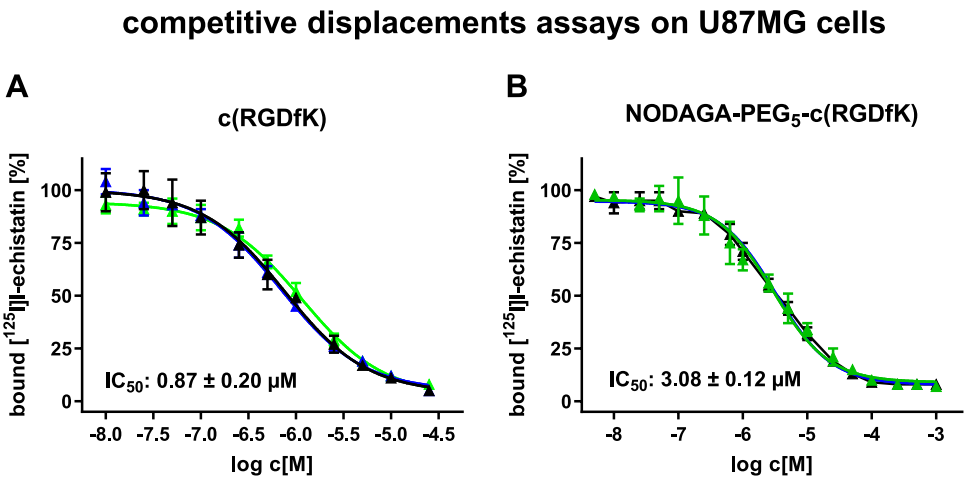

Figure 4. Graphical depiction of the results of the competitive displacements assays of the reference compound c(RGDfK) (A) and NODAGA-PEG_5-c(RGDfK) (B) on integrin $\alpha_v\beta_3$-positive U87MG tumor cells using [^{125}I]I-echistatin as the competitor. Each experiment was performed at least three times, each in triplicate. The curves obtained by the different experiments are depicted in different colors.

The synthesis of NODAGA-PEG_5-c(RGDfK) was followed by its radiolabeling with $^{68}Ga^{3+}$ to show the applicability of the developed agent for ^{68}Ga-labeling in high molar activity and radiochemical purity of the product and thus for [^{68}Ga]Ga-NODAGA-PEG_5-c(RGDfK) radiotracer production. For this purpose, 50−380 MBq of $^{68}Ga^{3+}$ were obtained in the form of [^{68}Ga]$GaCl_3$ by fractioned elution of a commercial ^{68}Ge/^{68}Ga-generator system and the pH of the solution was adjusted to 3.5−4.0 by the addition of sodium acetate. To this mixture, 1−20 nmol of NODAGA-PEG_5-c(RGDfK) precursor was added, and the solution was warmed to 45 °C for 10 min. Analytical radio-HPLC showed an almost quantitative formation of the product [^{68}Ga]Ga-NODAGA-PEG_5-c(RGDfK) (radiochemical yields and purities of ≥96% and molar activities of ≥41 GBq/μmol) (Figure 3C).

***In Vitro* Evaluation of Integrin $\alpha_v\beta_3$ Receptor Affinity of NODAGA-PEG_5-c(RGDfK) on U87MG Tumor Cells in 2D Monolayers.** In the development of new radiotracers for tumor imaging or therapy, the next step after the chemical synthesis of the precursors and their radiolabeling is the determination of the affinity of the new agents to the target structure, on the one hand, and the verification of their target specificity, on the other hand. Both characteristics are commonly studied using 2D human tumor cell monolayer-based assays on adherent cells. In particular, competitive displacement experiments are carried out to determine the affinity of the newly developed compounds in comparison to a known reference substance and, at the same time, to demonstrate the target specificity of the new agents. In the case of RGD peptides addressing the integrin $\alpha_v\beta_3$, human U87MG cancer cells are typically used for these studies as this glioblastoma cell line highly expresses the target structure and its use for this type of evaluation is well standardized.[18]

In order to define an internal standard for the following evaluations of spheroids, competitive displacement assays of NODAGA-PEG_5-c(RGDfK) on adherent U87MG cells were carried out first. In these experiments, [^{125}I]I-echistatin was used as the competitor and c(RGDfK) was applied as internal reference with known high affinity to this receptor type.[18] The results of these investigations are depicted in Figure 4, showing the binding curves obtained for reference compound c-(RGDfK) (Figure 4A) and NODAGA-PEG_5-c(RGDfK) (Figure 4B).

The reference demonstrated an integrin $\alpha_v\beta_3$-specific affinity with an IC_{50} value (half maximal inhibitory concentration) of 0.87 ± 0.20 μM which is in the typical range for this class of agents.[13,17] NODAGA-PEG_5-c(RGDfK) under the same conditions also displayed specific binding and an IC_{50} value of 3.08 ± 0.12 μM and thus a slightly lower affinity to the target compared to the lead compound, which is a common phenomenon observed for the modification of cyclic RGD peptides with a PEG linker and chelator.[19]

In addition to the target receptor affinities, the verification of integrin $\alpha_v\beta_3$-specific binding is important and also the low nonspecific interaction of the agents with the cells being reflected in the vast majority of the [^{125}I]I-echistatin being displaceable (low residual [^{125}I]I-echistatin activity on the cells of 5−8%). This is related to the specificity of the binding of the compounds present in the assay but also an indicator for the target receptors' accessibility on the 2D cells, resulting in an almost complete displaceability of [^{125}I]I-echistatin by c-(RGDfK) and NODAGA-PEG_5-c(RGDfK).

***In Vitro* Evaluation of Integrin $\alpha_v\beta_3$ Receptor Affinity of NODAGA-PEG_5-c(RGDfK) on U87MG 3D Tumor Cell Spheroids.** The receptor binding parameters of NODAGA-PEG_5-c(RGDfK) found in 2D cell monolayers were compared with those obtained in spheroidal 3D cell cultures. For this purpose, spheroids were generated of the U87MG cancer cells using the ultralow-attachment method, which is straightforward and generates highly comparable spheroids with a very low size variance of less than 5%.[20] Since potential supplementation-induced changes of the peptide binding characteristics or accessibility of the target structures should be investigated, different extracellular matrices (ECM) were used for spheroid generation.

First, one type of spheroids was generated in pure medium, i.e., without embedding in an extracellular matrix. Alternatively, two other types of spheroids were generated upon supplementation of the cells with collagen-1 or BME, both of which result in a hydrogel-like embedding of the cells and are the prevalently used matrices to support the formation of 3D cell cultures.[21,22] BME is an ECM extract harvested from the Engelbreth-Holm-Swarm sarcoma and can replace stromal

https://doi.org/10.1021/acsomega.4c08214
ACS Omega 2024, 9, 51349−51362

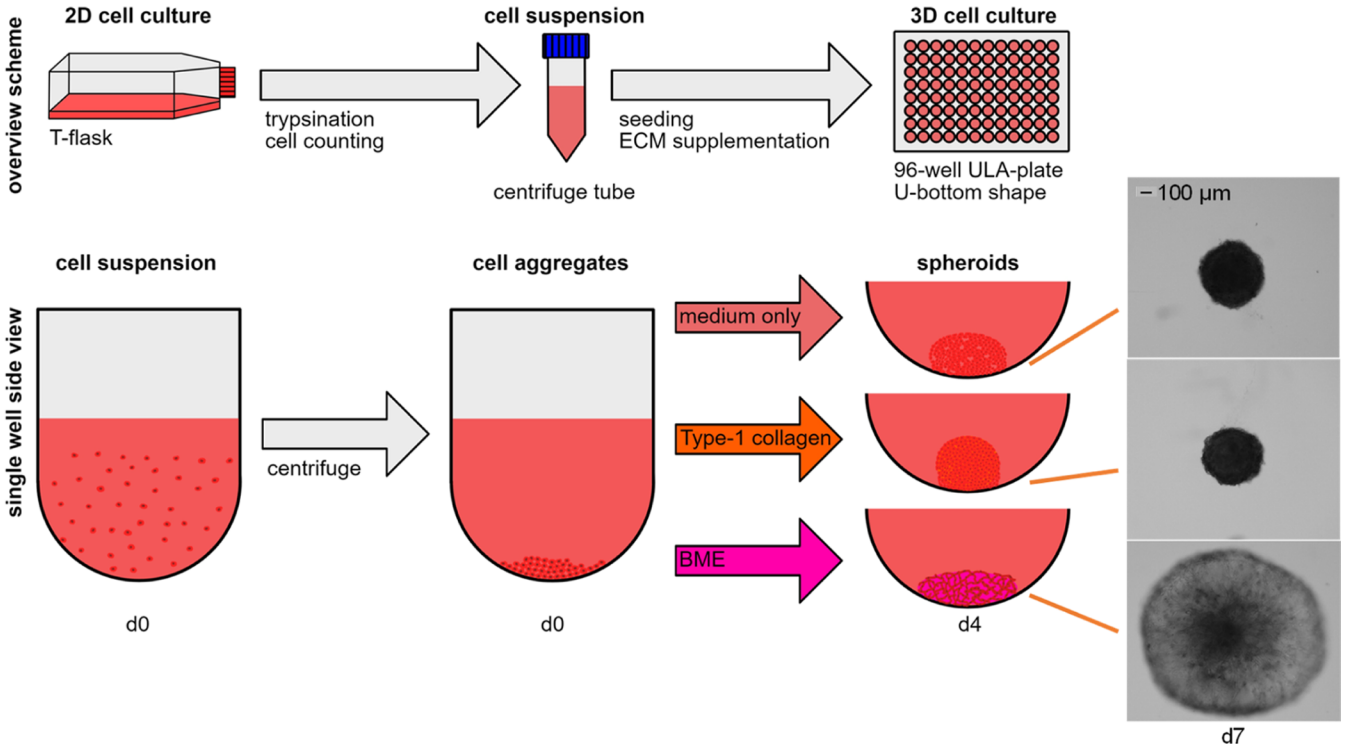

Figure 5. Schematic overview of the spheroid formation procedure. Starting from a regular 2D cell culture, cells were harvested with trypsin, collected in a centrifuge tube, and counted to define the cell concentration within the resulting suspension. Desired cell numbers were seeded into a 96-well plate with U-bottom shape and ultralow attachment (ULA) coating. After potential supplementation with an ECM compound, such as collagen-1 or basal membrane extract (BME) (if applicable), plates were centrifuged to facilitate cell aggregation. After 7 days of incubation under cell culture conditions, spheroid formation processes were complete and resulted in versatile morphologies (depicted on the right in the form of bright-field microscopy images of the U87MG spheroids at day 7 after seeding).

cells and other ECM components, whereas collagen-1 generates a matrix for 3D cell systems by forming protein-based hydrogels with a high affinity for various cells, mimicking the adhesive extracellular matrix in mature tissue. The generation of the different spheroid types is schematically depicted in Figure 5.

The spheroids—as expected[22,23]—markedly differed in size and morphology depending on the time and the matrix used for cultivation as determined by microscopy. Differences in cell growth and aggregation behavior could already be determined visually on day three after cell seeding and persisted over an observation period of 7 days (Figure 6).

The spheroids produced by these methods were used for the following investigations on the affinity of NODAGA-PEG$_5$-c(RGDfK) towards integrin $\alpha_v\beta_3$ by competitive displacement assays analogous to the 2D cell experiments described above. For this purpose, spheroids on day 7 after seeding were used, as their formation was complete by then. The results of these initial investigations are summarized in Figure 7 and show a significantly (about 5−7-fold) reduced interaction of NODAGA-PEG$_5$-c(RGDfK) with the cells in the 3D U87MG spheroids (IC_{50} values of 16.46 ± 2.88, 20.52 ± 4.41, and 18.44 ± 6.06 μM for spheroids generated without, collagen-1 and BME supplementation, respectively) compared to the 2D monolayer cell system (IC_{50}: 3.08 ± 0.12 μM, Figure 4).

Interestingly, the found IC_{50} values of NODAGA-PEG$_5$-c(RGDfK) to the target integrin were not affected by the matrix supplementation as in all three spheroid test systems, similar values were determined for nonembedded spheroids, collagen-1-supplemented and BME-supplemented spheroids, respectively. On the contrary, the results suggest that the presence and complexity of the matrix did not influence the interplay of NODAGA-PEG$_5$-c(RGDfK) and integrin $\alpha_v\beta_3$.

Nevertheless, a considerable decrease in the measured interaction of the ligand with the integrin was observed when compared with the results obtained using the 2D cell culture system. However, since the actual affinity of NODAGA-PEG$_5$-c(RGDfK) to the receptor is not likely to have changed, the decrease in the measured affinity must be due to other effects. One reason might be that the matrix used to generate the spheroids interacts directly with the receptor or the bound [^{125}I]I-echistatin and, by this, reduces the interaction with the receptor ligand. However, this is contradicted by the fact that similar IC_{50} values were observed with all spheroids, and thus similar integrin-matrix interactions would have had to take place for all spheroid types. This is however very unlikely, especially for the spheroids generated without the addition of additives. Another possibility is that the activation state of the receptor might have changed during the transition from 2D to 3D cell culture, thus reducing the interaction of the receptor ligand with the target. This effect would be independent of the matrix used and is therefore more likely, but cannot be proven here.

What appears to be most likely, though, is a reduction in receptor accessibility caused by the differing spatial arrangement of the cells, influencing the displacement of the bound [^{125}I]I-echistatin by the NODAGA-PEG$_5$-c(RGDfK) ligand. In particular, the accessibility of the inner cells of the spheroids should be significantly lower than at their surface compared to

https://doi.org/10.1021/acsomega.4c08214
ACS Omega 2024, 9, 51349−51362

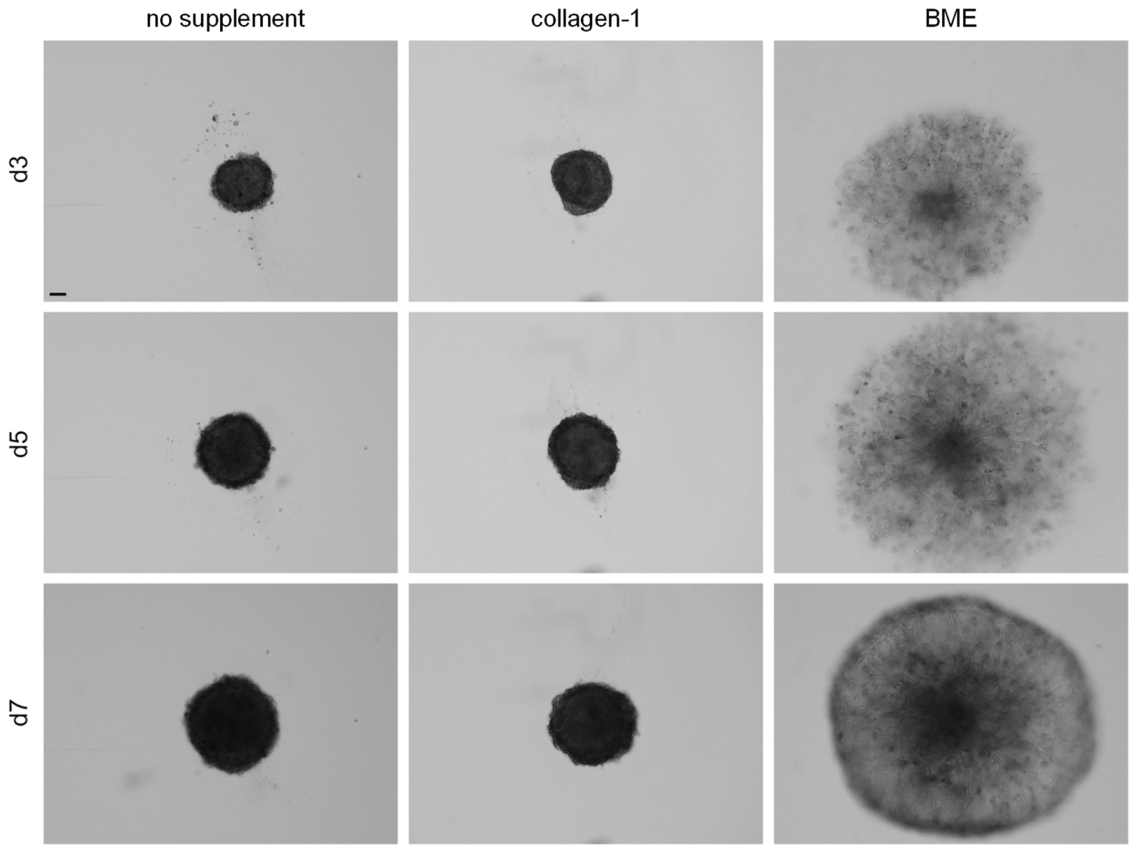

Figure 6. Representative bright-field microscopy images of spheroids at 3, 5, and 7 days after seeding of 2000 U87MG cells in 96-well ULA-plates containing media with different matrices or without supplementation (Cytation 5 microscope, scale: 100 μm).

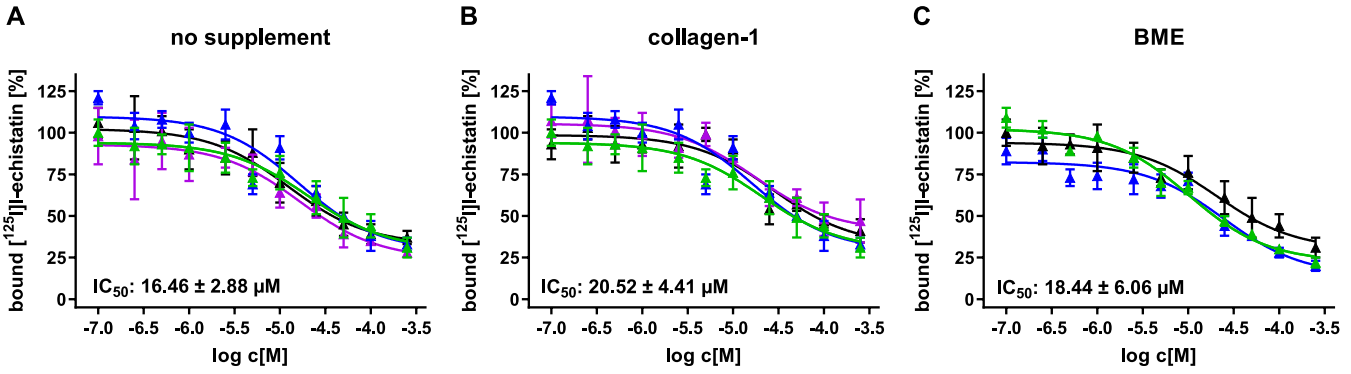

Figure 7. Graphical depiction of the results of the competitive displacements assays of NODAGA-PEG$_5$-c(RGDfK) on integrin $\alpha_v\beta_3$-positive U87MG tumor cell spheroids using [^{125}I]I-echistatin as the competitor. The assays were performed on spheroids generated without supplementation (A) and on spheroids obtained using collagen-1 (B) or BME supplementation (C). Each experiment was performed at least thrice, each in triplicate. The curves obtained by the different experiments are depicted in different colors.

2D cell monolayers, where cells and thus cell surface proteins are freely accessible from the apical side.

This assumption of a limited diffusion of NODAGA-PEG$_5$-c(RGDfK) into the spheroids combined with a limited cell and receptor accessibility and thus probability of [^{125}I]I-echistatin replacement would at least partly explain the significantly higher IC$_{50}$ values obtained in the spheroid models compared with the 2D cell monolayer. Fitting to the assumption that NODAGA-PEG$_5$-c(RGDfK)-integrin-interaction was sterically hindered/delayed by cell−cell interactions was the observed relatively high unspecific binding of [^{125}I]I-echistatin in the displacement assays on the 3D cell spheroids. This effect was most pronounced for the smaller and thus denser spheroids with collagen-1 supplementation (38.0 ± 7.4%) or without supplementary matrix (32.2 ± 3.8%) compared to the larger, less dense spheroids supplemented with BME (25.0 ± 5.2%) (Figure 6). Unspecific, nondisplaceable [^{125}I]I-echistatin activity in 2D cell monolayers was only between 5 and 8%. Thus, the density of the spheroids seems to be directly correlated with nondisplaceable binding as there was an inverse correlation between density of the spheroids and [^{125}I]I-echistatin displacement (Figure S1). This effect should be attributable to the diminished diffusion and thus accessibility of the integrin receptors in the case of the 3D spheroid systems compared to the 2D cell monolayers, since the affinity of the

https://doi.org/10.1021/acsomega.4c08214
ACS Omega 2024, 9, 51349−51362

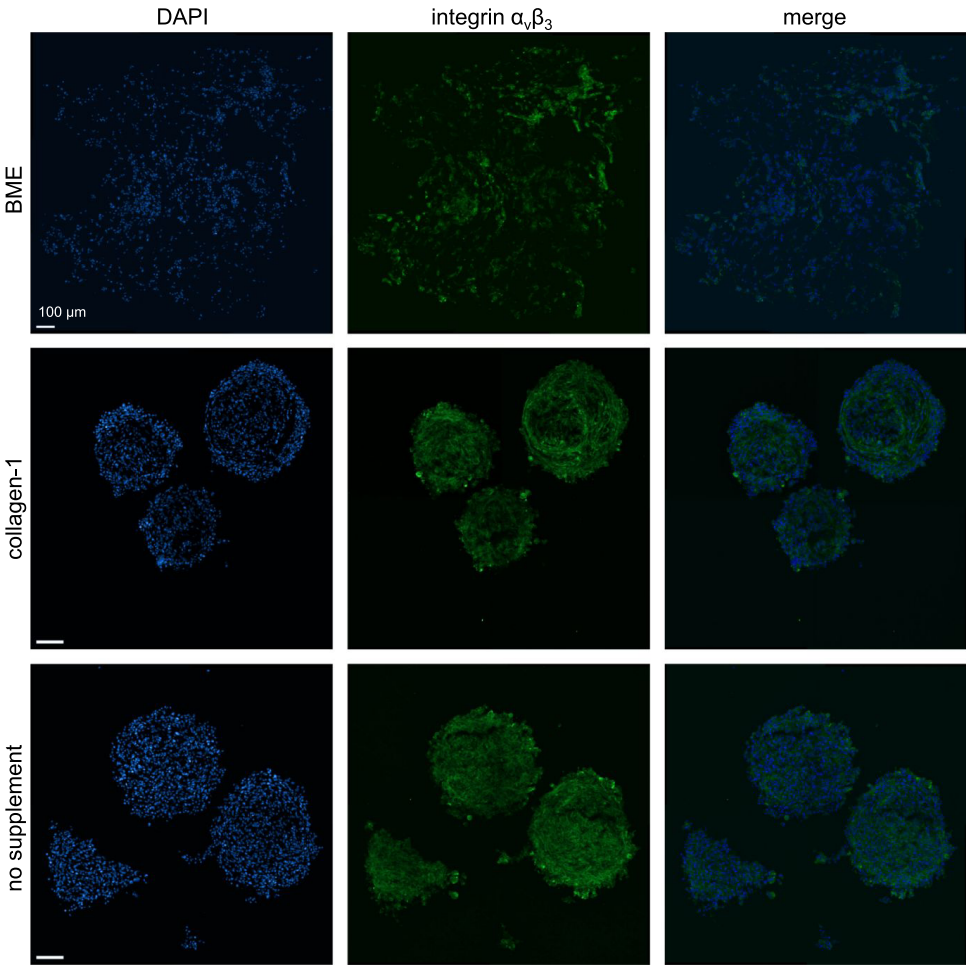

Figure 8. Representative fluorescence microscopy images of spheroids at day 7 after seeding of 2000 U87MG cells in 96-well ULA-plates containing media with different matrices or without supplementation. Spheroids were fixed and cut into 15 μm thick slices. Samples were stained for nuclei using DAPI (blue) and integrin $\alpha_v\beta_3$ using an $\alpha_v\beta_3$-specific primary antibody, followed by an antibody-specific secondary antibody (green). Representative sum projections of 20× confocal imaging Z-stacks covering the whole sample depth (scale: 100 μm, n = 3, 5 samples each). Brightness/contrast adjustments have been performed and within single marker pictures, pixels near saturations are shown in white for illustrative reasons only. Quantifications were performed independently based on raw data.

displacing ligand NODAGA-PEG$_5$-c(RGDfK) itself is not expected to vary between the different spheroid types.

Another point that supports these conclusions is the observation that the absolute uptake of [^{125}I]I-echistatin—with comparable amounts of radioligand applied, varies considerably between the spheroid types. While the small and highly dense spheroids that were generated without or collagen-1 supplementation took up only 3.4 ± 0.6% and 3.8 ± 0.8% of the total amount of [^{125}I]I-echistatin applied, the larger and less dense BME-supplemented spheroids showed an uptake of a significantly higher proportion of the total [^{125}I]I-echistatin amount added of 15.7 ± 2.8%. This clearly indicates that the high density of the small spheroids significantly limits the accessibility of and thus the interaction with the integrin receptors.

Since washing procedures in spheroid assays are always critical due to technical issues, removal of [^{125}I]I-echistatin by washing was potentially also limited in the 3D spheroid cultures and could therefore have further contributed to the higher nondisplaceable amount of activity observed in the 3D culture systems.

A prerequisite for the correctness of the assumption that the limited diffusion into the spheroids and thus the limited cell and surface receptor accessibility can be the reason for the higher IC$_{50}$ values obtained in the 3D spheroid models is however that all types of spheroids exhibit the same number of vital cells and accessible $\alpha_v\beta_3$ integrin binding sites.

Therefore, we further investigated the vitality of the tumor cells and the amount of accessible integrin $\alpha_v\beta_3$ within the different spheroid types. For this purpose, the spheroids without supplementation, with collagen-1, and with BME supplement were fixed in PFA, embedded within a cryomount, frozen at −80 °C and cut into 15 μm thick cryoslices. If apoptotic or necrotic cells were present within the spheroids, they should be located in the center due to the potentially insufficient supply of nutrients and oxygen in this area. Thus, the slices bearing the center of the respective spheroids were chosen for further processing and stained for nuclei and integrin $\alpha_v\beta_3$. The results of these experiments are depicted in Figure 8. They show ECM-dependent differences in cell densities but homogeneous marker distributions over the whole profile and no major signs of cell death such as cell rupture or apoptotic bodies. Thus, these data do not support the idea that apoptotic/necrotic processes were the reason for the observed differences in nonspecific binding between the

https://doi.org/10.1021/acsomega.4c08214
ACS Omega 2024, 9, 51349−51362

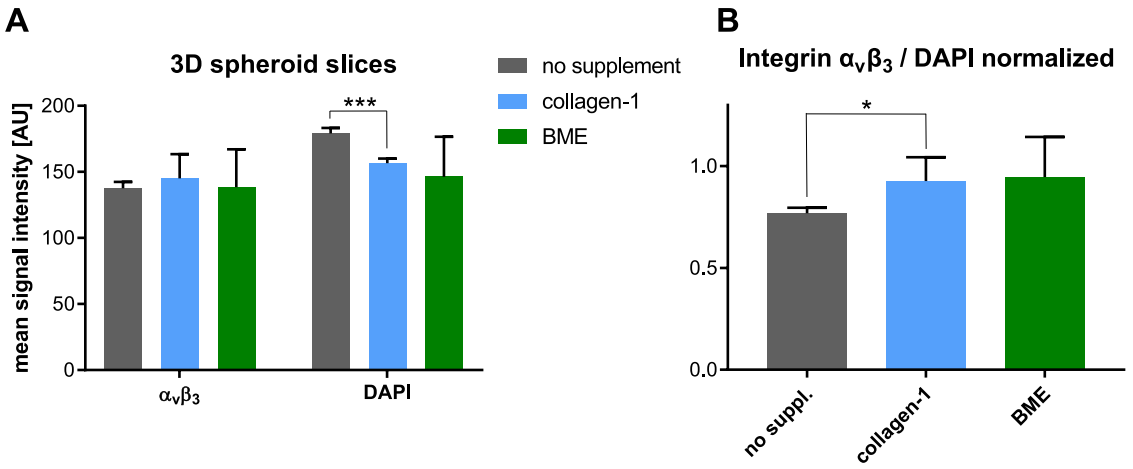

Figure 9. Quantitative analysis of the fluorescence signals of the integrin $\alpha_v\beta_3$-specific as well as the nuclear staining of the spheroids (A) and integrin $\alpha_v\beta_3$/DAPI ratio for the different spheroid types (B) (n = 3, 5 samples each).

spheroid types and the different IC_{50} values found for NODAGA-PEG_5-c(RGDfK) between 2D and 3D samples.

Since integrins are involved in cell−cell interaction, the amount of accessible integrin $\alpha_v\beta_3$ could also differ in a 3D cell spheroid from that in a 2D cell monolayer due to increased cellular interactions in a three-dimensional aggregate. This might result in the integrin molecules being involved in intercellular interactions and thus not or only restrictedly being accessible to ligand binding. Therefore, this aspect was also investigated. For this purpose, spheroids were sliced before staining and analysis to ensure complete staining and thus correct quantification of the target structures. Regarding the number of cells and accessible integrin proteins per spheroid, the investigations demonstrated significant differences between embedded and nonembedded spheroids. In detail, the spheroids without supplementation showed the highest DAPI signal intensities, whereas the integrin $\alpha_v\beta_3$-specific signal differed only insignificantly between spheroid types (Figure 9A). However, there was a trend that BME and collagen-1 supplementation increased the expression of integrin $\alpha_v\beta_3$ on the cell surface of spheroids (Figure 9B).

Although the collagen-1/BME-embedded spheroids showed a trend toward a higher expression of accessible integrin per cell compared to nonsupplemented spheroids (Figure 9B), an effect of the differential integrin expression of the different spheroid types on IC_{50} values should not be present as the replacement of an individual [^{125}I]I-echistatin molecule from the receptor by a NODAGA-PEG_5-c(RGDfK) molecule should not be influenced by the number of accessible $\alpha_v\beta_3$ integrins. Further, the quantitative analysis of the total integrin content per spheroid type (Figure S2) demonstrated only insignificant differences between the spheroid types (total integrin signal per spheroid type of 24 623 ± 886, 22 693 ± 2877, and 20 234 ± 4204 for spheroids without supplementation, collagen-1 and BME supplementation, respectively). This indicates that the total amount of integrin receptors being present on the different 3D structures being comparable is not expected to have influenced the determined IC_{50} values.

Taken together, apoptotic/necrotic effects or differing integrin contents in the spheroid types are unlikely to have had a major effect on the determination of IC_{50} values on the spheroids, highlighting that limited accessibility of the target proteins due to either steric effects or the agents used for supplementation were more critical.

Effect of ECM Composition on Ligand−Receptor Interaction in U87MG Monolayers. In order to assess the role of matrix proteins in the unspecific binding of integrin-specific agents, we further studied the influence of the two additives collagen-1 and BME on cells cultured in 2D monolayers. For this purpose, U87MG cells were cultured under standard conditions, harvested, and seeded in medium containing no additive, collagen-1, or BME in 24-well plates containing glass coverslips. After 30 min of incubation at 37 °C, samples were washed, fixed with PFA, and stained for nuclei, integrin $\alpha_v\beta_3$, and actin for internal control. The fluorescence microscopy images and the quantification of the accessible amount of integrin per cell in these experiments are shown in Figures 10A,B and S3.

These data suggest that the amount of accessible integrin in monolayer cultures was significantly altered already after short-term cultivation in a BME-comprising medium compared to cells not receiving additional supplementation. Since it is unlikely that the expression of integrin already changed in this short time frame, it follows that the accessibility of/interaction with the integrin was altered by BME. This is supported by the results of a competitive binding assay in the absence or the presence of the same amount of BME as it was used in the 3D spheroid assays (2.5 vol % of BME in basal medium). Indeed, as depicted in Figure 10C, a significant influence of the BME on the binding behavior of the NODAGA-PEG_5-c(RGDfK) was observed, as it resulted in a triplication of the determined IC_{50} value to 10.39 ± 0.89 μM (without BME supplementation, the IC_{50} value was measured to be 3.08 ± 0.12 μM). In contrast, no such effect could be shown for collagen-1 (Figure 10B) which is in line with the literature describing interactions between collagen-1 and various integrins ($\alpha_1\beta_1$, $\alpha_2\beta_1$, $\alpha_{10}\beta_1$, and $\alpha_{11}\beta_1$) but not with integrin $\alpha_v\beta_3$.[24]

This implies that BME impairs the displacement of [^{125}I]I-echistatin by the integrin-specific ligand, either by reducing the accessibility of the receptor or by interacting with the receptor or ligand itself or bound [^{125}I]I-echistatin, impairing its displacement. The matrix used, as well as the cellular density of the spheroids, therefore has a significant influence on the obtained results of the evaluation of ligand−receptor interactions. This highlights the importance of a high degree of standardization/optimization of tumor cell spheroid generation if diagnostic radiopharmaceuticals are to be

https://doi.org/10.1021/acsomega.4c08214
ACS Omega 2024, 9, 51349−51362

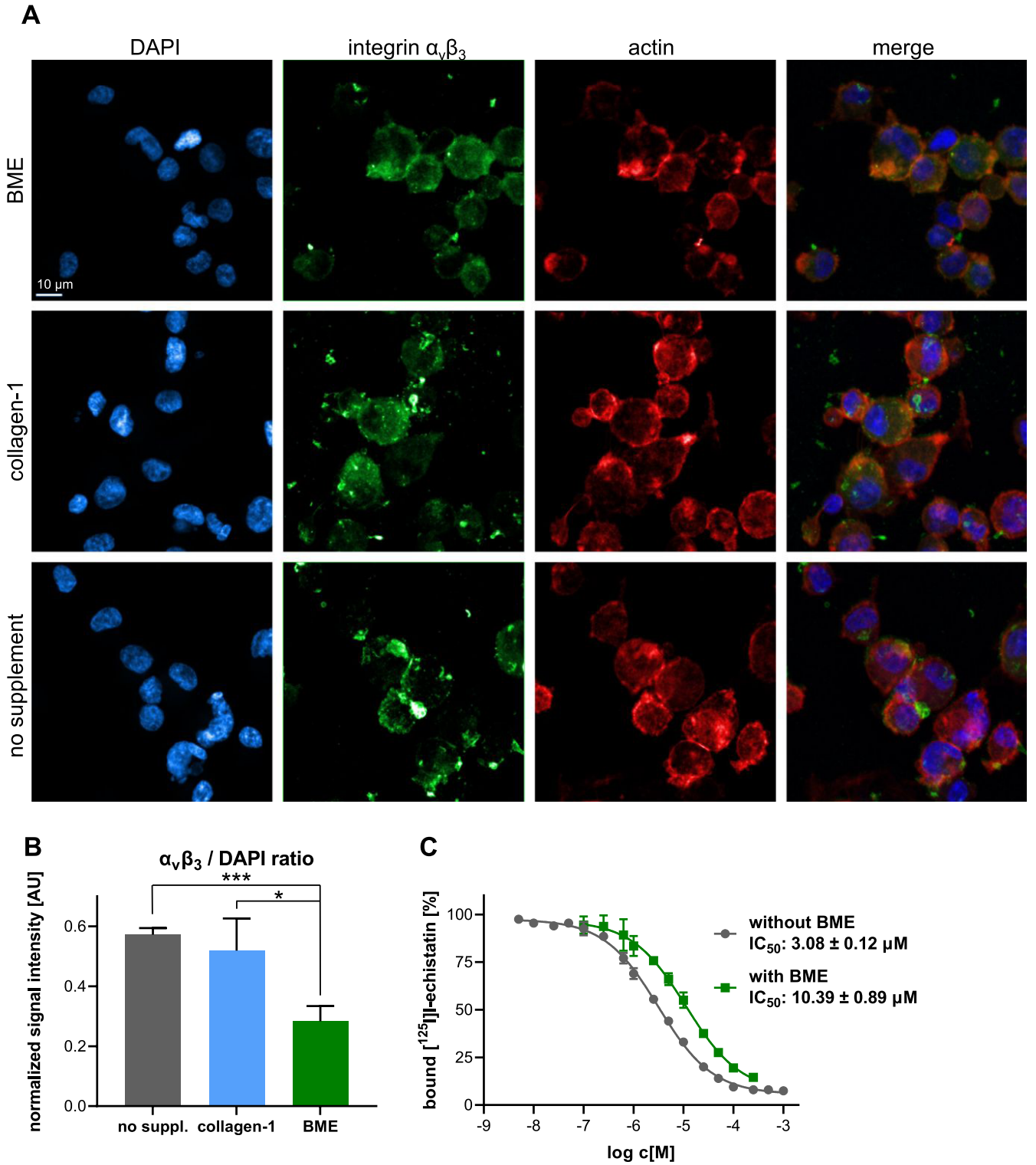

Figure 10. Analyses on U87MG cells in 2D monolayers. (A) Representative fluorescence microscopy images of U87MG cells after short-term incubation with different additives (collagen-1 or BME) or without supplementation. For this purpose, cells were harvested, suspended in media containing the supplements as indicated, and seeded in 24-well plates containing glass coverslips. After 30 min of incubation (37 °C/5% CO_2/humidified atmosphere), samples were washed, and after PFA fixation stained for nuclei (DAPI/blue), integrin $\alpha_v\beta_3$ (green), or actin (red; used as internal control). Shown are representative sum projections of 63× confocal imaging Z-stacks covering the whole sample depth to illustrate marker distributions (scale: 10 μm, n = 3 × 3 samples each). Brightness/contrast adjustments have been performed and within single marker pictures, pixels near saturations are shown in white for illustrative reasons only. Quantifications were performed independently based on raw data. (B) Quantitative analysis of integrin $\alpha_v\beta_3$/DAPI ratio for the different cell supplementation procedures (n = 3 × 3 samples each). (C) Results of the competitive displacements assays of NODAGA-PEG_5-c(RGDfK) on U87MG cells without supplementation or in medium containing BME as a supplement using [^{125}I]I-echistatin as the competitor. Each experiment was performed at least thrice, each in triplicate.

https://doi.org/10.1021/acsomega.4c08214
ACS Omega 2024, 9, 51349−51362

investigated with regard to their target-specific binding properties in these systems.

CONCLUSIONS

Taken together, in a direct comparison between 2D monolayer and 3D spheroid cell culture of U87MG cancer cells, we found significant differences in the results of competitive displacement assays, determined IC_{50} values and also unspecific binding of integrin $\alpha_v\beta_3$-specific agents. Ligand−receptor interaction was decreased, and unspecific binding was increased in spheroids compared to cell monolayers. The subsequently performed studies suggest that these effects can be mainly attributed to a lower accessibility of/interaction with the integrin target protein in the 3D spheroid model due to masking of the receptor by matrix components and reduced diffusion of agents to the inner cells of the spheroids. In contrast, apoptotic/necrotic effects as well as different integrin contents in the different spheroid types were, as expected, not found to be drivers for the observed effects.

Although the results of this study are not strictly transferable to the evaluation of other receptor-specific binding substances, different receptor types, and tumor cells as they might behave differently in transition from 2D monolayer cell culture to 3D spheroids, some general conclusions can be drawn from this study. Above all, the results demonstrate that the evaluation of diagnostic radioligands on tumor cell spheroids is rather complex and dependent on many factors. Although spheroid systems used for testing of therapeutic radioligands provide very valuable predictive information on the therapeutic response under *in vivo* conditions going beyond the results obtainable in 2D cell culture, 2D monolayer tumor cell systems represent a very well-standardized model for assessing the affinity of newly designed diagnostic radioligands to their respective target receptor.

In contrast, spheroid models could be very useful to study *in vitro* the diffusion/infiltration of diagnostic radioligands into the tumor and by this to potentially predict uptake under *in vivo* conditions. This aspect is not investigated at all in the comparative testing of new diagnostic radioligands so far but may, of course, significantly influence the *in vivo* PET imaging results. Further research is thus needed in this direction, and the present work demonstrates the high importance of standardization/optimization in the process of spheroid generation and the implementation of the *in vitro* experiments.

METHODS

General Information on Chemical and Radiochemical Syntheses and Instrumentation. *Chemicals and Radiochemicals.* All chemicals were purchased from commercial sources in analytical grade quality and used without further purification unless otherwise stated. Fmoc- and side-chain-protected amino acids, Fmoc-Asp(Nova Syn TGA)-OAll resin (loading 0.18−0.21 mmol/g) as well as benzotriazol-1-yloxytripyrrolidinophosphonium hexafluorophosphate (PyBOP) were purchased from NovaBiochem (Darmstadt, Germany). 4-(4,7-Bis(2-(*t*-butoxy)-2-oxoethyl)-1,4,7-triazacyclononan-1-yl)-5-(tert-butoxy)-5-oxo-pentanoic acid ((R)-NODA-GA(^{t}Bu)$_3$) was purchased from CheMatech (Dijon, France). 18-(9-Fluorenylmethyloxycarbonylamino)-4,7,10,13-tetraoxa-octadecanoic acid (Fmoc-NH-PEG$_5$-COOH) was obtained from Iris Biotech (Marktredwitz, Germany). Dichloromethane (DCM), diethyl ether, dimethylformamide (DMF), piperidine, 2-(1*H*-benzotriazol-1-yl)-1,1,3,3-tetramethyluronium hexafluorophosphate (HBTU), trifluoroacetic acid (TFA), and water were purchased from Carl Roth (Karlsruhe, Germany); acetonitrile (MeCN) from Häberle Labortechnik (Lonsee-Ettlenschieß, Germany); and *N*,*N*-diisopropylethylamine (DIPEA) and triisopropylsilane (TIS) from Sigma-Aldrich (Taufkirchen, Germany). [^{125}I]I-Echistatin was purchased with a molar activity of 81.4 TBq/mmol from Revvity (former PerkinElmer, Rodgau, Germany; custom synthesis NEX083000MC). $^{68}GaCl_3$ for the ^{68}Ga-radiolabeling reactions was obtained from a Galli Ad ^{68}Ge/^{68}Ga-generator system (IRE ELIT, Fleurus, Belgium). Acetic acid (glacial) was purchased from Thermo Fisher Scientific (Darmstadt, Germany) while sodium acetate, water (Tracepur quality), hydrochloric acid (30%, Suprapur quality), and sodium hydroxide (30%, Suprapur quality) for radiolabeling reactions were purchased from Merck (Darmstadt, Germany). 4-(2-Hydroxyethyl)piperazine-1-ethanesulfonic acid (HEPES, ultrapure quality) was obtained from Gerbu Biotechnik GmbH (Heidelberg, Germany). c(RGDfK) was synthesized as described before.[16]

Materials for In Vitro Assays. U87MG cells were obtained from ATCC (Wesel, Germany), and MultiScreen$_{HTS}$-BV 1,2 μm 96-well plates from Merck Chemicals (Darmstadt, Germany). Cultrex BME was purchased from Bio-Techne GmbH (Wiesbaden, Germany). Eagle's Minimum Essential Medium (EMEM) was obtained from ATCC (Wesel, Germany); trypsin solution (0.25%) and penicillin-streptomycin (10 000 U/mL) from Thermo Fisher Scientific (Darmstadt, Germany); and fetal calf serum (FCS) from Bio&SELL (Feucht, Germany).

Instrumentation. HPLC: Analytical HPLC, semipreparative HPLC, and analytical radio-HPLC were conducted utilizing a Dionex UltiMate 3000 system together with Chromeleon Software (Version 6.80). For analytical chromatography, Chromolith Performance (RP-18e, 100−4.6 mm, Merck, Germany) and, for semipreparative analyses, Chromolith SemiPrep (RP-18e, 100−10 mm, Merck, Germany) columns were used, respectively. For radioanalytical chromatography, a Dionex UltiMate 3000 system equipped with a Raytest GABI* radioactivity detector was used together with a Chromolith Performance (RP-18e, 100−4.6 mm, Merck, Germany) column. All operations were performed with a flow rate of 4 mL/min using H_2O supplemented with 0.1% TFA and MeCN also supplemented with 0.1% TFA as solvents. MALDI-TOF MS: matrix-assisted laser desorption/ionization (MALDI) time-of-flight (TOF) mass spectra were obtained utilizing a Bruker Daltonics Microflex spectrometer (Bremen, Germany), linear acquisition mode, positive ion source, and 200 shots per spot. α-Cyano-4-hydroxycinnamic acid (α-CS) was chosen as matrix and the dried-droplet method was used for sample preparation on a micro scout target (MSP 96 target polished steel BC, Bruker Daltonics, Germany). The data were recorded with flexControl v 3.3 and analyzed with flexAnalysis Version 3.3 software (Bruker Daltonics, Bremen, Germany). HR-ESI-MS: For high-resolution electrospray ionization mass spectroscopy (HR-ESI-MS), a Thermo Finnigan LTQ FT Ultra Fourier Transform Ion Cyclotron Resonance (Dreieich, Germany) mass spectrometer was used. The resolution was adjusted to 100.000 at m/z 400. Depending on the sample, a mass range of 50−2000 u was chosen. The spray capillary voltage at the IonMax ESI-nozzle was 4 kV, the temperature of the heater capillaries was 250 °C, the nitrogen sheath gas flow

https://doi.org/10.1021/acsomega.4c08214
ACS Omega 2024, 9, 51349−51362

was 20, and the sweep gas flow was 5 units. Flow injection analysis (FIA/ESI) utilized a surveyor MS pump at a flow rate of 100 μL/min with water/acetonitrile (2:8, *v*/*v* or 8:2, *v*/*v*) as solvent. 1−10 μL of the sample were injected under use of an inline filter. γ-Counter: γ-Counting was performed using a 2480 Wizard[2] γ counter system from PerkinElmer. Ultrasonic bath: Ultrasound-assisted syntheses were performed in a Bandelin Sonorex Super RK 225 H ultrasonic bath (Berlin, Germany) with the temperature of the water kept at ambient temperature.

Synthesis of NODAGA-PEG$_5$-c(RGDfK). NODAGA-PEG$_5$-c(Arg-Gly-Asp-D-Phe-Lys) was synthesized utilizing a commercially available Fmoc-Asp(Nova Syn TGA)-OAll resin (loading 0.18−0.21 mmol/g, 27 μmol) according to standard amino acid coupling protocols using commonly applied N_α-Fmoc amino acids, Fmoc-Lys(Mtt)-OH, Fmoc-NH-PEG$_5$-COOH, (*R*)-NODA-GA(^{t}Bu)$_3$ together with HBTU as coupling reagent and DIPEA as base for activation. The linear peptide sequence Arg-Gly-Asp-D-Phe-Lys was synthesized according to standard protocols.[16,25] For this purpose, conventional syringes (5 mL, HSW, Tuttlingen, Germany) equipped with two layers of 35 μm porous high-density polyethylene frits (Reichelt Chemietechnik, Heidelberg, Germany) were used for the manual syntheses, with the resin being placed between the plunger and frits. Directly before coupling of the first amino acid, the resin was swollen for 30 min in DCM and washed thrice with DMF afterward to exchange the solvent. Coupling reactions were carried out in DMF for 15 min in an ultrasonic bath at ambient temperature using 2 equiv of the respective amino acid and 1.9 equiv of HBTU as the coupling reagent with 2 equiv of DIPEA as the base. The removal of Fmoc-protecting groups was performed with 50% piperidine in DMF (*v*/*v*) for 2 and 5 min, respectively. The OAll-protecting group of the asparagine was removed with Pd(PPh$_3$)$_4$ (0.25 equiv, 6.75 μmol, 7.8 mg) and phenylsilane (24 equiv, 648 μmol, 79.8 μL) in DCM (3 min × 30 min) and the subsequent cyclization of the linear peptide was performed on the resin by the addition of HBTU (1 equiv, 27 μmol, 10.2 mg) and DIPEA (1 equiv, 27 μmol, 3.5 μL) for 1 h. The Mtt-protecting group of the lysine was removed with TFA in DCM (2/98, *v*/*v*) within 25 min (5 min × 5 min), followed by 3-fold washing of the resin with first DCM and afterward DIPEA in DCM (1:9, *v*/*v*). Fmoc-NH-PEG$_5$-COOH was conjugated according to the standard procedure, while (*R*)-NODA-GA(^{t}Bu)$_3$ was conjugated by utilizing PyBOP instead of HBTU as the coupling reagent and a prolonged reaction time of 30 min. Product cleavage from the resin and removal of acid-labile protecting groups was performed with a mixture of TFA, TIS, and H$_2$O (95:2.5:2.5, *v*/*v*/*v*) for 3 h at room temperature. The volatile materials were evaporated, and the crude product was dissolved in 1:1 MeCN/H$_2$O + 0.1% TFA (*v*/*v*), purified by semipreparative HPLC (gradient: 0−40% MeCN + 0.1% TFA in 8 min (R_t = 6.61 min)), and the pure product lyophilized subsequently. The product was obtained as a white fluffy solid after lyophilization in a yield of 34.7% over all steps. MALDI-TOF-MS (*m*/*z*) using α-cyano-4-hydroxycinnamic acid as matrix substance for $[M + H]^+$ (calculated): 1296.26 (1296.67). HR-ESI-MS (*m*/*z*) $[M + 2H]^{2+}$ (calculated): 648.8370 (648.8377), $[M + H]^+$ (calculated): 1296.6688 (1296.6682), $[M - H]^-$ (calculated): 1294.6522 (1294.6536).

^{68}Ga-Radiolabeling of the Precursor, Yielding [^{68}Ga]Ga-NODAGA-PEG$_5$-c(RGDfK). For the radiolabeling of NODAGA-PEG$_5$-c(RGDfK) with $^{68}Ga^{3+}$, [^{68}Ga]GaCl$_3$ was obtained by the elution of a commercial ^{68}Ge/^{68}Ga-generator system (Galli Ad, IRE Elit). A 1 mM solution of the peptide (1−20 nmol) in H$_2$O (Tracepur quality) was added to a solution of 50−380 MBq of [^{68}Ga]GaCl$_3$ (0.47−1.1 mL) in 0.1 M HCl and the pH was adjusted to 3.5−4.0 by adding sodium acetate solution (pH 4.6, 1.25 M, 230−540 μL). After 10 min incubation at 45 °C on a thermoshaker, radiochemical purity was determined via analytical radio-HPLC. The radiolabeled product was found to be ≥96% pure and obtained in nonoptimized molar activities of ≥41 GBq/μmol.

Cell Culture. *2D Cell Culture (Cell Monolayers).* U87MG primary human glioblastoma cells were kept in Eagle's Minimum Essential Medium (EMEM; ATCC, 30−2003) supplemented with 10% (*v*/*v*) fetal bovine serum (FCS; Capricorn, FBS-12A) and 1% (*v*/*v*) penicillin/streptomycin (10 000 U/mL, Gibco) at 37 °C in a humidified CO$_2$ (5%) atmosphere and were split at >80% confluency.

3D System Generation (Spheroids). Spheroids were generated in ultralow-attachment plates (ULA plate; FaCellitate, Biofloat 96-well, F202003) by seeding 2000 cells within a total volume of 150 μL of media with the corresponding supplementation status (no additive/Coll1/BME). After centrifugation at 500 rcf for 7 min, culture plates were cultivated for 4 days, before a 50 μL exchange of medium was carried out, and after 7 days, further investigations were performed in the competitive displacement assays or via PFA fixation for 1 h at ambient temperature for consecutive fluorescence staining. Size monitoring was performed with bright-field microscopy (Zeiss Axiovert 25/CP-ACHROMAT, 5×/0.12Ph0 objective and Agilent BioTek Cytation 5) followed by semiautomated analysis with the SpheroidSizer software.[26]

Competitive Displacement Studies in 2D and 3D Cell Culture Systems. MultiScreen$_{HTS}$-BV, 1,2 μm 96-well plates were conditioned for 1 h with BSA/PBS (1:99, *w*/*v*) solution (200 μL per well) before use. Each well was seeded with 1.5 × 10^5 U87MG cells (2D experiments) or three spheroids of the three different cell spheroid types (3D, obtained without matrix or with collagen-1 or BME as matrix), suspended in EMEM containing 20 mM Tris, pH 7.4, and supplemented with 150 mM NaCl, 2 mM CaCl$_2$, 1 mM MgCl$_2$, 1 mM MnCl$_2$, and 0.1% BSA/EMEM containing 20 mM Tris, pH 7.4, and supplemented with 150 mM NaCl, 2 mM CaCl$_2$, 1 mM MgCl$_2$, 1 mM MnCl$_2$, 0.1% BSA, and BME (2.5 vol %, 100 μL) (2D monolayer/3D spheroid experiments) and incubated at 37 °C for 0.5 h. To each well, 0.25 kBq [^{125}I]I-echistatin (25 μL) was added in the presence of 11 increasing concentrations, ranging from 5 × 10^{-9} to 10^{-3} M (2D monolayer experiments without supplementation) or 10^{-7} to 2.5 × 10^{-4} M (all other assays) NODAGA-PEG$_5$-c(RGDfK) (25 μL) with one well not receiving the agent ensuring 100% binding of the radioligand. After 1 h of incubation, the supernatant was removed, and the filters were washed three times with cold PBS (1 × 200 μL, 2 × 100 μL) to remove unbound [^{125}I]I-echistatin, collected, and measured in a γ-counter. The 50% inhibitory concentration (IC_{50}) values for each compound were obtained by nonlinear regression analysis using GraphPad Prism Software (v5.04). Each experiment was performed at least three times, each experiment being performed in triplicate.

Confocal Microscopy. *3D Systems (Spheroids).* For confocal microscopy imaging, fixed samples were processed

https://doi.org/10.1021/acsomega.4c08214
ACS Omega 2024, 9, 51349−51362

as previously described.[27] In brief, spheroids were embedded within a frozen section compound (Leica, FSC 22 Clear, 3801480) mounted on self-designed cryo-molds made of gelatin for easier processing of parallelized samples.[28] After sectioning on a cryostat (Leica CM 1950) and the transfer of the 15 μm thick slices on slides (epredia, Superfrost Plus, J1800AMNZ), samples were kept frozen at −80 °C prior to further processing in parallel with the 2D samples. Therefore, all staining samples were permeabilized using a mixture of 10% DMSO, 0.3 M glycine, and 0.2% Triton X-100 in PBS for 30 min at ambient temperature and afterward blocked using a mixture of 10% DMSO, 1% BSA, and 0.2% Triton X-100 in PBS for 1 h at ambient temperature before incubating with the corresponding antibodies and dyes in a buffer consisting of 5% DMSO, 1% BSA, 0.2% Tween 20, and 10 μg/mL heparin in PBS (Dulbecco's Phosphate Buffered Saline, D8537). Primary antibody incubation of the anti-$\alpha_V\beta_3$ antibody (1:200; Sigma-Aldrich, ZRB1190, rabbit monoclonal at 4 °C overnight) was followed by washing (3 min × 5 min with PBS) and sample exposition for 2 h at ambient temperature to the same basal buffer containing the secondary antibody (donkey antirabbit Alexa-Fluor-555, 1:1000; Invitrogen, A32794) and the dyes for actin (SirActin, 1:1000; tebubio, SC001; SiR-actin Kit) as well as for nuclei (DAPI, 1:1000; Roche, 10236276001). After final washing, samples were mounted using Mowiol and the imaging was performed on a Leica SP8 microscope equipped with HC PL APO 20×/0.75 IMM CORR and HC PL APO CS2 63×/1.2 W CORR objectives and the Las-X 3.3.0 software with Glycerol immersion media (RI = 1.450; Leica Microsystems, 11513910). Quantitative 20× objective pictures were taken at 1024 × 1024 pixel resolution on Z-stacks covering the whole sample body at 2 μm step size. After background correction, sum projections were obtained using the ImageJ software (version 1.54f), and foreground pixel mean intensities were measured within regions of interest. Qualitative 63× objective pictures were taken at 2048 × 2048 pixel resolution with 2.0 zoom and 0.25 μm step size. All data acquisitions were performed with 3× frame and 2× line averaging to reduce background detection.

2D System (Cell Monolayers). For 2D investigations, sterilized coverslips (12 mm; VWR; ECN 631-1577) were placed in 24-well plates (Greiner, 662160). To match the radioactive screening protocol, cells were trypsinated, centrifuged, and resuspended in media only or media supplemented with either 5 μg/mL Collagen Type-1 (Coll1; Roche, 11179179001) or 2.5% basal membrane extract (BME; Biotechne, Cultrex PathClear BME, 3432-005-01) before seeding 900 000 cells per well in 600 μL volume. After 30 min at 37 °C, supernatants were removed, and the samples were washed with PBS before PFA fixation (4% in PBS for 1 h at ambient temperature).

Statistics. For statistics of the immunostainings, GraphPad Prism 7 software was used. For 3D spheroid samples, data analysis was performed with one-way ANOVA without assumptions following the Holm-Sidak procedure of unpaired column analysis based on optional single-ample normalization. For 2D monolayer samples, Gaussian distribution was ensured by analyzing the mean of mean signals (2D monolayer) in one-way ANOVA considering homoscedasticity. For direct comparison of two data sets, significance was defined by P-values (*: $P < 0.05$, **: $P < 0.01$, ***: $P < 0.001$, ****: $P < 0.0001$) in multiple comparison t tests.

■ ASSOCIATED CONTENT

Data Availability Statement

The data underlying this study are available in the published article and its Supporting Information.

Supporting Information

The Supporting Information is available free of charge at https://pubs.acs.org/doi/10.1021/acsomega.4c08214.

Comprising an illustration of the correlation between the size and density of the spheroids and the observed unspecific binding of [^{125}I]I-echistatin; quantitative analysis of the total integrin content per spheroid type; and fluorescence microscopy images of U87MG cells after short-term cultivation with different additives or without supplementation (PDF)

■ AUTHOR INFORMATION

Corresponding Author

▽**Carmen Wängler** − *Heidelberg University, Medical Faculty Mannheim, Biomedical Chemistry, 68167 Mannheim, Germany; Medical Faculty Mannheim, Research Campus M^{2}OLIE, Heidelberg University, 68167 Mannheim, Germany;* orcid.org/0000-0003-1161-8669; Email: Carmen.Waengler@uni-heidelberg.de

Authors

Benedikt Judmann − *Heidelberg University, Medical Faculty Mannheim, Biomedical Chemistry, 68167 Mannheim, Germany; Medical Faculty Mannheim, Research Campus M^{2}OLIE, Heidelberg University, 68167 Mannheim, Germany*

Florian Keller − *Medical Faculty Mannheim, Research Campus M^{2}OLIE, Heidelberg University, 68167 Mannheim, Germany; Mannheim University of Applied Sciences, CeMOS, 68163 Mannheim, Germany;* orcid.org/0000-0003-3745-6872

Björn Wängler − *Medical Faculty Mannheim, Research Campus M^{2}OLIE and Medical Faculty Mannheim, Molecular Imaging and Radiochemistry, Heidelberg University, 68167 Mannheim, Germany*

Ralf Schirrmacher − *Department of Oncology, Division of Oncological Imaging, University of Alberta, Edmonton, Alberta, Canada T6G 1Z2;* orcid.org/0000-0002-7098-3036

▽**Rüdiger Rudolf** − *Medical Faculty Mannheim, Research Campus M^{2}OLIE, Heidelberg University, 68167 Mannheim, Germany; Mannheim University of Applied Sciences, CeMOS, 68163 Mannheim, Germany*

Complete contact information is available at: https://pubs.acs.org/10.1021/acsomega.4c08214

Author Contributions

#B.J. and F.K. contributed equally. B.J.: Conceptualization; data curation; formal analysis; methodology; visualization; writing—original draft. F.K.: Conceptualization; data curation; formal analysis; methodology; visualization; writing—original draft. B.W.: Formal analysis; writing—review and editing. R.S.: Formal analysis; writing—review and editing. R.R.: Conceptualization; formal analysis; methodology; project administration; supervision; writing—original draft; writing—review and editing. C.W.: Conceptualization; formal analysis; methodology; project administration; supervision; writing—original draft; Writing—review and editing.

https://doi.org/10.1021/acsomega.4c08214
ACS Omega 2024, 9, 51349−51362

Funding

This research project is part of the Forschungscampus M²OLIE and funded by the German Federal Ministry of Education and Research (BMBF) within the Framework "Research Campus—public-private partnership for Innovation" under the funding codes 13GW0389B and 13GW0388A.

Notes

The authors declare no competing financial interest.

[▽]R.R. and C.W. share senior authorship.

■ ACKNOWLEDGMENTS

The authors thank Dr. Werner Spahl (LMU Munich) for performing the HR-ESI mass spectroscopy.

■ REFERENCES

(1) Mohtavinejad, N.; Ardestani, M. S.; Khalaj, A.; Pormohammad, A.; Najafi, R.; Bitarafan-Rajabi, A.; Hajiramezanali, M.; Amanlou, M. Application of radiolabeled peptides in tumor imaging and therapy. *Life Sci.* **2020**, *258*, No. 118206.

(2) Kręcisz, P.; Czarnecka, K.; Królicki, L.; Mikiciuk-Olasik, E.; Szymanski, P. Radiolabeled Peptides and Antibodies in Medicine. *Bioconjugate Chem.* **2021**, *32*, 25−42.

(3) Jensen, C.; Teng, Y. Is It Time to Start Transitioning From 2D to 3D Cell Culture? *Front. Mol. Biosci.* **2020**, *7*, 33.

(4) Azimian Zavareh, V.; Rafiee, L.; Sheikholeslam, M.; Shariati, L.; Vaseghi, G.; Savoji, H.; Javanmard, S. H. Three-Dimensional in Vitro Models: A Promising Tool To Scale-Up Breast Cancer Research. *ACS Biomater. Sci. Eng.* **2022**, *8*, 4648−4672.

(5) Pinto, B.; Henriques, A. C.; Silva, P. M. A.; Bousbaa, H. Three-Dimensional Spheroids as In Vitro Preclinical Models for Cancer Research. *Pharmaceutics* **2020**, *12*, 1186.

(6) Hirschhaeuser, F.; Menne, H.; Dittfeld, C.; West, J.; Mueller-Klieser, W.; Kunz-Schughart, L. A. Multicellular tumor spheroids: An underestimated tool is catching up again. *J. Biotechnol.* **2010**, *148*, 3−15.

(7) Doctor, A.; Seifert, V.; Ullrich, M.; Hauser, S.; Pietzsch, J. Three-Dimensional Cell Culture Systems in Radiopharmaceutical Cancer Research. *Cancers* **2020**, *12*, 2765.

(8) Neshasteh-Riz, A.; Angerson, W. J.; Reeves, J. R.; Smith, G.; Rampling, R.; Mairs, R. J. Incorporation of iododeoxyuridine in multicellular glioma spheroids: implications for DNA-targeted radiotherapy using Auger electron emitters. *Br. J. Cancer* **1997**, *75*, 493−499.

(9) Zschenker, O.; Streichert, T.; Hehlgans, S.; Cordes, N. Genome-Wide Gene Expression Analysis in Cancer Cells Reveals 3D Growth to Affect ECM and Processes Associated with Cell Adhesion but Not DNA Repair. *PLoS One* **2012**, *7*, No. e34279.

(10) Niu, G.; Chen, X. Y. Why Integrin as a Primary Target for Imaging and Therapy. *Theranostics* **2011**, *1*, 30−47.

(11) Brooks, P. C.; Clark, R. A.; Cheresh, D. A. Requirement of Vascular Integrin Alpha(V)Beta(3) for Angiogenesis. *Science* **1994**, *264*, 569−571.

(12) Li, L.; Chen, X. Y.; Yu, J. M.; Yuan, S. H. Preliminary Clinical Application of RGD-Containing Peptides as PET Radiotracers for Imaging Tumors. *Front. Oncol.* **2022**, *12*, No. 837952.

(13) Liu, S. Radiolabeled Cyclic RGD Peptide Bioconjugates as Radiotracers Targeting Multiple Integrins. *Bioconjugate Chem.* **2015**, *26*, 1413−1438.

(14) Cukierman, E.; Pankov, R.; Stevens, D. R.; Yamada, K. M. Taking cell-matrix adhesions to the third dimension. *Science* **2001**, *294*, 1708−1712.

(15) Weigelt, B.; Lo, A. T.; Park, C. C.; Gray, J. W.; Bissell, M. J. HER2 signaling pathway activation and response of breast cancer cells to HER2-targeting agents is dependent strongly on the 3D microenvironment. *Breast Cancer Res. Treat.* **2010**, *122*, 35−43.

(16) Braun, D.; Judmann, B.; Cheng, X.; Wängler, B.; Schirrmacher, R.; Fricker, G.; Wängler, C. Synthesis, Radiolabeling, and In Vitro and In Vivo Characterization of Heterobivalent Peptidic Agents for Bispecific EGFR and Integrin alpha v beta 3 Targeting. *ACS Omega* **2023**, *8*, 2793−2807.

(17) Cheng, X.; Hubner, R.; von Kiedrowski, V.; Fricker, G.; Schirrmacher, R.; Wängler, C.; Wängler, B. Design, Synthesis, In Vitro and In Vivo Evaluation of Heterobivalent SiFAlin-Modified Peptidic Radioligands Targeting Both Integrin alpha(v)beta(3) and the MC1 Receptor-Suitable for the Specific Visualization of Melanomas? *Pharmaceuticals* **2021**, *14*, 547.

(18) Kapp, T. G.; Rechenmacher, F.; Neubauer, S.; Maltsev, O. V.; Cavalcanti-Adam, E. A.; Zarka, R.; Reuning, U.; Notni, J.; Wester, H. J.; Mas-Moruno, C.; Spatz, J.; Geiger, B.; Kessler, H. A Comprehensive Evaluation of the Activity and Selectivity Profile of Ligands for RGD-binding Integrins. *Sci. Rep.* **2017**, *7*, No. 39805.

(19) Chen, X. Y.; Hou, Y. P.; Tohme, M.; Park, R.; Khankaldyyan, V.; Gonzales-Gomez, I.; Bading, J. R.; Laug, W. E.; Conti, P. S. Pegylated Arg-Gly-Asp peptide: Cu labeling and PET imaging of brain tumor $\alpha v\beta 3$-integrin expression. *J. Nucl. Med.* **2004**, *45*, 1776−1783.

(20) Breslin, S.; O'Driscoll, L. Three-dimensional cell culture: the missing link in drug discovery. *Drug Discovery Today* **2013**, *18*, 240−249.

(21) Habanjar, O.; Diab-Assaf, M.; Caldefie-Chezet, F.; Delort, L. 3D Cell Culture Systems: Tumor Application, Advantages, and Disadvantages. *Int. J. Mol. Sci.* **2021**, *22*, 12200.

(22) Keller, F.; Rudolf, R.; Hafner, M. Towards optimized breast cancer 3D spheroid mono- and co-culture models for pharmacological research and screening. *J. Cell Biotechnol.* **2019**, *5*, 89−101.

(23) Calori, I. R.; Alves, S. R.; Bi, H.; Tedesco, A. C. Type-I Collagen/Collagenase Modulates the 3D Structure and Behavior of Glioblastoma Spheroid Models. *ACS Appl. Bio Mater.* **2022**, *5*, 723−733.

(24) Pang, X. C.; He, X.; Qiu, Z. W.; Zhang, H. X.; Xie, R.; Liu, Z. Y.; Gu, Y. L.; Zhao, N.; Xiang, Q.; Cui, Y. M. Targeting integrin pathways: mechanisms and advances in therapy. *Signal Transduction Targeted Ther.* **2023**, *8* (1), No. 1.

(25) Wängler, C.; Maschauer, S.; Prante, O.; Schafer, M.; Schirrmacher, R.; Bartenstein, P.; Eisenhut, M.; Wängler, B. Multimerization of cRGD Peptides by Click Chemistry: Synthetic Strategies, Chemical Limitations, and Influence on Biological Properties. *ChemBioChem* **2010**, *11*, 2168−2181.

(26) Chen, W. J.; Wong, C.; Vosburgh, E.; Levine, A. J.; Foran, D. J.; Xu, E. Y. High-throughput Image Analysis of Tumor Spheroids: A User-friendly Software Application to Measure the Size of Spheroids Automatically and Accurately. *J. Visualized Exp.: JoVE* **2014**, No. e51639.

(27) Keller, F.; Bruch, R.; Schneider, R.; Meier-Hubberten, J.; Hafner, M.; Rudolf, R. A Scaffold-Free 3-D Co-Culture Mimics the Major Features of the Reverse Warburg Effect In Vitro. *Cells* **2020**, *9*, 1900.

(28) Iakab, S. S.; Keller, F.; Schmidt, S.; Cordes, J.; Zhou, Q.; Cairns, J. L.; Fischer, F.; Schneider, R.; Wolf, I.; Rudolf, R.; Hopf, C. 3D-Mass Spectrometry Imaging of Micro-scale 3D Cell Culture Models in Cancer Research *bioRxiv* 2022, p 2022-12.

https://doi.org/10.1021/acsomega.4c08214
ACS Omega 2024, 9, 51349−51362